Control of the spatial emission structure of broad-area vertical-cavity surface-emitting lasers by feedback

2009 J. Phys. D: Appl. Phys. 42 055101

(http://iopscience.iop.org/0022-3727/42/5/055101)

IOP PUBLISHING JOURNAL OF PHYSICS D: APPLIED PHYSICS

J. Phys. D: Appl. Phys. **42** (2009) 055101 (9pp) doi:10.1088/0022-3727/42/5/055101

Control of the spatial emission structure of broad-area vertical-cavity surface-emitting lasers by feedback

M Schulz-Ruhtenberg[1], Y Tanguy[2], K F Huang[3], R Jäger[4] and T Ackemann[2]

[1] Institut für Angewandte Physik, Westfälische Wilhelms-Universität Münster, Corrensstrasse 2/4, 48149 Münster, Germany
[2] SUPA and Department of Physics, University of Strathclyde, Glasgow G4 0NG, UK
[3] Department of Electrophysics, National Chiao Tung University, Hsinchu, Taiwan
[4] Philips Technologie GmbH, U-L-M Photonics, Lise-Meitner-Str. 13, 89081 Ulm, Germany

E-mail: thorsten.ackemann@strath.ac.uk

Received 22 July 2008, in final form 8 December 2008
Published 5 February 2009
Online at stacks.iop.org/JPhysD/42/055101

Abstract
The wave number of transverse spatial structures in broad-area vertical-cavity surface-emitting lasers (VCSELs) is controlled via frequency-selective feedback from an external self-imaging cavity in a broad range of wave numbers and emission frequencies. The selected states follow the dispersion curves of the free-running laser. A control range of about 2.5 μm^{-1} in spatial frequency space and 2.5 nm in emission wavelength was obtained for square VCSELs and of about 3 μm^{-1} and 8 nm for circular VCSELs having a different dispersion curve. By spatial filtering in Fourier space, the shape of the structures can also be controlled to some extent. It is argued that the feedback techniques are useful to 'probe' emission states of the free-running laser.

(Some figures in this article are in colour only in the electronic version)

1. Introduction

Broad-area edge-emitting semiconductor lasers are very attractive compact and monolithic sources for material processing, medical applications and laser pumping though their brilliance is limited due to a rather poor spatial and temporal coherence (e.g. [1]). Broad-area vertical-cavity surface-emitting lasers (VCSELs) are less developed but potentially even more attractive due to their non-elliptical beam profile and single-longitudinal mode behaviour [2, 3]. However, due to the fact that the single pass gain is low due to the wavelength-scale cavity length, achieving high power VCSELs necessarily demands a large extent of the transverse aperture. The resulting high Fresnel number implies that high power VCSELs are prone to transverse instabilities and multi-transverse mode behaviour. In addition, dynamical instabilities down to picosecond time scales have to be expected (e.g. [4–6]) and were indeed observed in edge-emitting lasers [7].

Due to these dynamical instabilities present in free-running lasers there is profound interest in control schemes. A very powerful tool is optical feedback, in many cases in conjunction with filtering techniques [6, 8–13]. Promising progress was achieved in controlling the emission of broad-area edge-emitting semiconductor lasers [11, 13–19]. Some of these works also witnessed interest in stabilizing other spatial distributions than the fundamental/homogeneous mode as long as the mode stability and thus the temporal coherence can be improved. In VCSELs, the stabilization of the fundamental mode as well as some high order modes was demonstrated in a small Fresnel number situation where Gaussian modes were emitted [20]. It was also shown that small bistable microlasers—a special type of spatial dissipative soliton—can be stabilized within a broad-area VCSEL with frequency-selective feedback [21, 22].

Additional motivation for the control of broad-area lasers stems from the general thrust for control techniques for

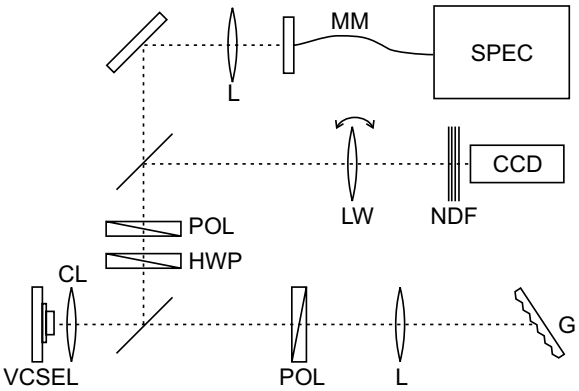

Figure 1. Schematic setup: CL—collimation lens, POL—linear polarizer, HWP—half-wave retardation plate, L—lens, G—grating, LW—lens wheel, NDF—neutral density filters, CCD—charge-coupled-device (CCD) camera, MM—multi-mode fiber, SPEC—spectrometer.

spatial extended systems in the framework of nonlinear dynamics. Though some approaches exist in different chemical and physical systems, these investigations are just at their starting point (e.g. [23]). In nonlinear optics a Fourier space based feedback technique was suggested for nonlinear resonators [24] motivating many successful implementations in single-mirror feedback schemes [25–28].

In this contribution we utilize a scheme based on a broad-area VCSEL with frequency-selective feedback. Since in plano-planar resonators the frequency and wave number are coupled [9, 29, 30], the square of the wave number being proportional to the detuning between emission frequency and the longitudinal cavity resonance, frequency control also provides wave number control (and vice versa, e.g. [9]). We briefly discuss the effect of spatial filtering in Fourier space and a combination of frequency and spatial filtering. We illustrate that feedback can be used to 'probe' the structures of the free-running laser in some sense providing a further example for the usefulness of feedback in understanding the mode structure and behaviour of the unperturbed system [24, 27].

2. Experimental setup

The experimental setup is shown schematically in figure 1. The devices under study are oxide-confined top-emitting VCSELs emitting at around 780 nm as described in [30, 31]. Their square apertures have a cross-section of $a = 40\,\mu$m. The cavity, consisting of three 8 nm thick $Al_{0.1}Ga_{0.9}As$ quantum wells and $Al_{0.4}Ga_{0.6}As$ spacer layers, is sandwiched by two highly reflective distributed Bragg reflectors (DBRs, top mirror: 31 layers, bottom mirror: 47.5 layers). For comparison, in some experiments circular oxide-confined bottom-emitting VCSELs with a diameter of 80 μm and an emission wavelength of 980 nm were investigated. Their epitaxial structure is similar to the ones described in [3, 21].

The VCSEL is driven by a low-noise current source. The laser is mounted onto a Peltier element-controlled heat sink with a feedback circuit. Due to the fact that the wavelengths of the gain maximum and of the cavity resonance shift with different rates with temperature, the heat sink temperature controls the detuning condition in a single-longitudinal mode laser [29, 30, 32]. The wavenumber of the threshold mode has a square-root shaped dependence on detuning due to the resonant properties of plane–plane cavities [29, 30]. The minimum temperature to be investigated is limited to about 10 °C, where water starts to condense at the cold side of the heat sink. At 10 °C the wave number at threshold emitted from the free-running VCSELs under study is about 2.5 μm^{-1}. Thus a lens with a relatively low numerical aperture (NA) is sufficient to collimate the laser beam allowing for the use of a relatively high focal length, which in turn facilitates the placement of a beam splitter between the lens and its Fourier plane. An aspheric lens with a focal length $f = 11$ mm and an NA of 0.3 is used. The Fresnel reflection of a glass substrate with anti-reflection coating on one side is used to split off a small portion (1–10% depending on the polarization direction) of the beam for the detection arm.

In the feedback beam path a second lens (focal length 300 mm) is used to image the plane of the active zone of the laser onto the feedback grating or mirror, which in turn retro-reflects the beam into the VCSEL. This system is self-imaging, i.e. has an ABCD-transfer matrix $\left(\begin{smallmatrix}1 & 0\\ 0 & 1\end{smallmatrix}\right)$ [21]. This is the only configuration which can support arbitrary field distributions. For example, a telescopic system with three lenses and a transfer matrix $\left(\begin{smallmatrix}-1 & 0\\ 0 & -1\end{smallmatrix}\right)$ was found to yield only inversion symmetric structures (as expected). Geometric imaging of the VCSEL aperture onto the feedback element results in a round-trip transfer matrix having a non-zero value in the non-diagonal component coupling position to angle (i.e. describing focusing). Due to the fact that the VCSEL resonance depends on the incidence angle, this will change the feedback conditions (see the discussion below, equation (3)).

For frequency-selective feedback a holographic grating with 1800 lines mm^{-1} is used. The grating is used in Littrow configuration [33], i.e. the first order of the grating is reflected back into the VCSEL. The diffraction efficiency of the grating is highly anisotropic favouring horizontal polarization. In order to have completely defined polarization conditions, a polarizer is inserted into the feedback arm and set for transmission of the horizontal component.

In the detection arm a high-resolution digital CCD camera is used to record the intensity distributions in near and far fields. The half-wave plate in combination with the linear polarizer is used to analyse the polarization of the emission. The fact that the reflection coefficient of the intra-cavity beam splitter is about ten times higher for vertically polarized light than for linearly polarized light needs to be taken into account when the polarization properties are characterized. The Fourier images of the laser emission taken with the CCD camera are calibrated from pixels to divergence angles or wave numbers by measuring the angle directly with the camera placed in front of the laser without any imaging optics for some values of parameters in free-running operation.

In addition, a grating spectrograph with a resolution of 0.07 nm is used to measure the wavelength of the emission. For all experiments the feedback was adjusted with great care using the threshold reduction (i.e. the difference between the

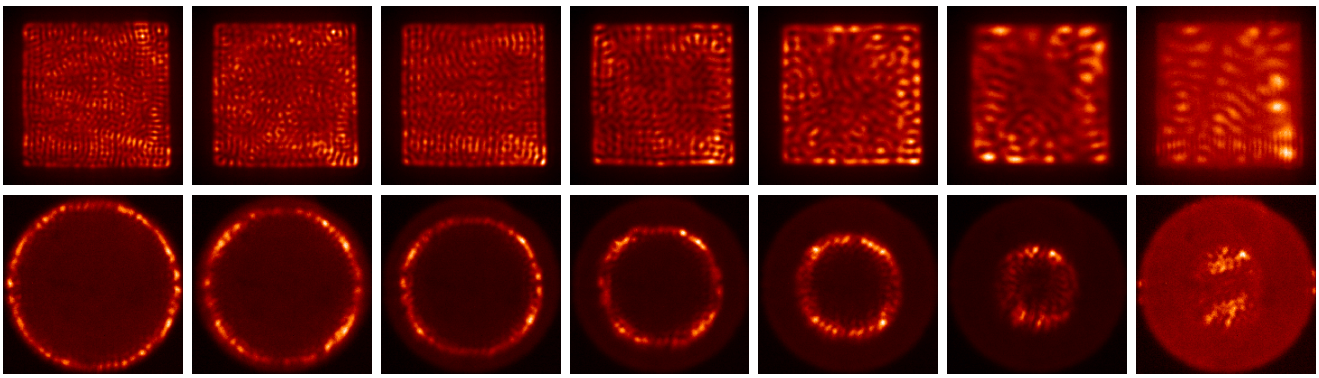

Figure 2. (Colour online) Near-field (upper row) and far-field (lower row) intensity distributions of the laser under the influence of frequency-selective feedback. From left to right the grating is rotated so that the feedback frequency is reduced. The frequency step between the images is about −120 GHz or 0.24 nm. The intensity increases from black to white in a greyscale (print version) or a temperature (online version) coding. The range displayed in the near field is 52 μm, in the far field $\pm 2.6\,\mu\mathrm{m}^{-1}$.

laser threshold of the free-running device and the threshold with feedback) and the increase in the output power above threshold as criteria (the monitoring photodetector not shown in the setup). With frequency-selective feedback a maximum threshold reduction of up to 20% was measured.

3. Experimental results: control of length scales

In a first experiment the feedback frequency is changed by rotating the grating in steps of about 0.01° (by shifting a differential screw in steps of 12.5 μm). Accordingly the feedback frequency is changed by −74 GHz (or 0.15 nm in wavelength). The laser is operated around the threshold, so that without feedback no significant lasing emission is detected.

In the optical spectra measured with the spectrograph a quasi-continuous shift of the emitted wavelength is apparent. The frequency of laser emission simply follows the changing feedback frequency with a linear relationship. The slope is 0.96. We do not think that this is a systematic deviation from the expected value of 1 but due to the uncertainty in determining the length of the lever arm from the pivot point of the grating holder to the point where the screw acts.

So far, the behaviour corresponds to that of a grating-controlled external cavity laser conventionally used for spectroscopy. An examination of the spatial structures, however, shows profound differences (figure 2). It is obvious that the dominant pattern length scale is reduced during the scan towards smaller wavelengths: the near-field intensity distribution on the far left shows a finely modulated pattern, the ring in the far field has a radius of 2.4 $\mu\mathrm{m}^{-1}$, close to the maximum transmitted by the collimation lens. On the far right the pattern has a much larger wavelength; the wave number has shrunk accordingly.

For all settings of the feedback the far field shows a single continuous ring with some seemingly irregular modulations. A tendency to some distinct enhancement is present at the diagonals. The polarization is found to be horizontal in all regions of high intensity in near and far fields as expected from the fact that the feedback favours horizontally polarized states.

Figure 3 shows the dependence of the wave number on the wavelength at two temperatures. The wavelength is expressed

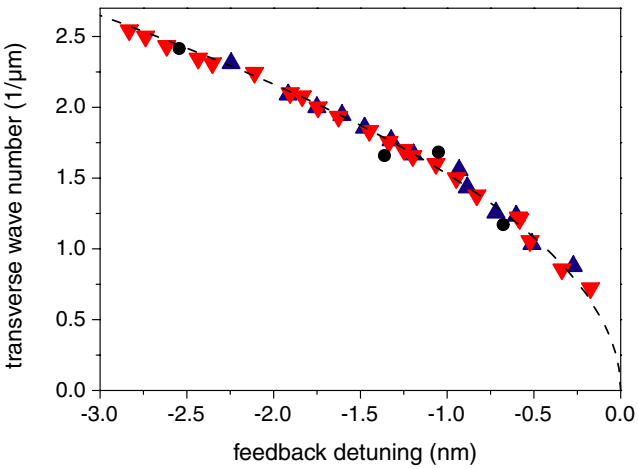

Figure 3. (Colour online) Plot of the dependence of the transverse wave number on the emission wavelength imposed by the frequency-selective feedback expressed as detuning to the longitudinal resonance. The grey (red online) down-triangles correspond to a heat sink temperature of 10 °C, the black (blue online) up-triangles to 20 °C. The dashed black line is a fit to the corresponding data of all our lasers under free-running conditions (i.e. from data as the ones in figure 7 of [30] but based on more data). The circular, black data points are the modes which are realized in the free-running laser close to threshold, if the heat sink temperature is varied.

as the detuning with respect to the longitudinal cavity resonance obtained from an interpolation procedure [30]. The temperature-induced shift of the cavity resonance conditions is corrected by measuring the dependence of the emission wavelength on the heat sink temperature and the current for a single mode.

The first important observation is that the data points lie on the same—square-root shaped [29, 30]—dispersion curve as the modes of the free-running laser (given by the dashed black line; as mentioned in section 2 in the free-running laser it can be measured by changing the temperature of the heat sink). This indicates that the external cavity is sufficiently close to the self-imaging condition as to not alter the dispersion of the spatial states and hence the states selected by the feedback are modes of the free-running laser or superpositions thereof.

The second observation is that the data do not depend on the heat sink temperature though the free-running laser emits at a wave number of 3.0 μm^{-1} at 10 °C and of 1.7 μm^{-1} at 20 °C. This demonstrates that the control by feedback is effective for different operating conditions of the free-running laser. The wave number where the maximum emission is achieved depends on the heat sink temperature determining the detuning between the gain line and the longitudinal cavity resonance. As expected, it is higher (at 1.8 μm^{-1}) at 10 °C than at 20 °C (1.1 μm^{-1}). Contrary to expectation, the maximum amplitude with feedback is not found at the wave number at which the free running is operating. The reason for this is not clear. One might suspect that the losses in the feedback loop increase for increasing wave numbers but this conclusion is not supported by the results reported in figure 6 in section 4.

Feedback control is effective over a range of wavelength of about 2.5 nm and wave number 0.8–2.5 μm^{-1}. At the small wavelength/large wave number side the limit is given by the NA of the lens in the current implementation and hence might be extended by using a lens with a higher NA, though probably not significantly because the amplitude of the emissions already drops considerably compared with the maximum (achieved in the range 1.6–2.1 μm^{-1}).

On the high wavelength/low wave number side, the laser investigated here stops at a detuning of about −0.3 nm and a wave number of 0.8 μm^{-1}. In other lasers on-axis emission centred around $k_\perp = 0$ can be selected. This would be the preferred state for applications but the benefit is limited because the emission is not homogeneous in near field (or, more precisely, corresponding to the fundamental mode of the transverse waveguide formed by the oxide aperture of the VCSEL), but 'spots' or 'filaments' with a diameter of typically a few micrometres. The same states are emitted by the free-running laser at higher heat sink temperatures (see figure 5(*a*) of [30], figure 1(*a*) of [31], figure 3(*a*) of [32]). They are probably related to inhomogeneities across the transverse aperture of the laser inhibiting 'true homogeneous' states.

Figure 3 shows that the wave number can be tuned by feedback in a much more continuous way than in the free-running laser by changing the heat sink temperature (circular data points). The next neighbour wavelength separation with feedback is about 0.07–0.15 nm. This is of the order of the discretization imposed by the boundary conditions. In one spatial dimension, it corresponds to $\Delta k_\perp = \pi/a$ (a size of the laser aperture), which leads to a discretization in wavelength of about 0.16 nm. Obviously, in two dimensions, there are more wave numbers allowed than in 1D and the spacing in wavelength can be smaller. These observations show that the feedback enables the emission of transverse modes that are not observed without feedback (at least close to the threshold). One concludes that there need to be spectral variations in the gain or loss curves for the free-running laser favouring particular wave numbers, but that the feedback strength is stronger than these variations so that the states can be excited by feedback.

We mention further that typically the free-running lasers emit a ring in Fourier space with homogeneous polarization for low enough wave numbers (up to about 1.5–2 μm^{-1} depending on the device, denoted as region I in [31]) whereas they switch to a symmetry broken four peak structure at a higher wave number (denoted as region II in [31]). In region I, the polarization is selected by unavoidable material anisotropies, in the second by an interplay of the reflection at the oxide waveguide and the DBRs (see [31]). With feedback, the regime of region I seems to be extended.

For an interpretation of the results, it is useful to recall that within linear approximation a change in incidence angle implies an equal but opposite change in the diffraction angle at the Littrow wavelength (i.e. the wavelength where the first diffraction order of a beam coming in on the optical axis is retro-reflected into the incoming beam),

$$\mathrm{d}\beta = -\mathrm{d}\alpha, \tag{1}$$

where α is the incidence angle of the beam onto the grating and β the diffraction angle (both measured with respect to the grating normal). This can be easily derived from the grating equation

$$g(\sin\alpha + \sin\beta) = \lambda, \tag{2}$$

where g denotes the grating period and λ the wavelength of the light. This means that at the Littrow wavelength, the grating behaves like an ordinary mirror aligned perpendicular to the optical axis (see figure 4(*a*) for an illustration). Since the external cavity is self-imaging, any intensity distribution at that wavelength receives feedback. The square-root-like dispersion curve due to the resonance condition for plane waves in the VCSEL cavity (dashed black line in figure 3) fixes a one-to-one correspondence between the wavelength and the transverse wave number. Hence, if the feedback selects a wavelength, the transverse wavenumber is also selected. This argument also explains why the dispersion relation of the feedback-selected modes matches the one of the free-running VCSEL.

The frequency selectivity of the scheme stems from the fact that a ray with a wavelength detuned from the Littrow condition will return to the VCSEL at an angle different from the original one (figure 4(*b*)), though still to the same position. Figure 4(*b*) shows an on-axis wave as an example but the same change in angle occurs for any off-axis wave. Hence, the returning ray does not match the resonance condition of the VCSEL (does not fit the dispersion curve) any longer and is rejected. We will develop a more quantitative treatment below.

Typically, the spectral emission width is about 0.1–0.3 nm, i.e. the wavelength (and wave number) is quite well defined by the feedback but nearly all of the individual spectra are not single frequency. It seems that the range of frequencies reflected by the grating and focused back into the laser is larger than this mode spacing. Indeed, it can be estimated to be 0.4 nm from the standard argument that the resolution of a grating is proportional to the number of illuminated grooves and the selected state is assumed to extend over the whole aperture of the laser. In the feedback scheme investigated here, it is also necessary to check for the angular dispersion after the beam diffracted by the grating is recaptured by the intra-cavity lens system. As indicated, under self-imaging conditions a ray with a wavelength detuned from the Littrow condition comes back

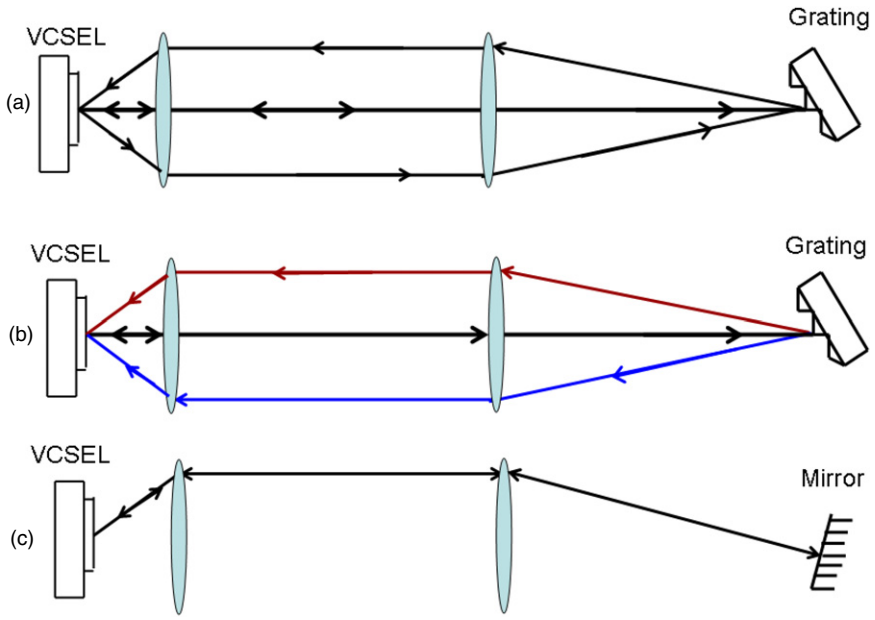

Figure 4. (Colour online) Schemes of ray trajectories in the external cavity. (*a*) The path of a ray at the Littrow wavelength closes into itself independent of its propagation angle with respect to the optical axis. (*b*) A ray with a wavelength different from the Littrow wavelength propagating towards the grating along the optical axis (black lines) is coming back at the same location but at a different angle. The sign of deviation depends on whether it is blue-detuned (lower ray path, blue online) or red-detuned (upper ray path, red online) with respect to the Littrow wavelength. (*c*) A tilted mirror retro-reflects rays arriving at the tilt angle into itself. Note that there is no reproduction of the ray after one round trip unless some mechanism in the VCSEL coupled rays at equal but opposite angles.

still to the same position after a round trip but at a different angle. To first order, the angular dispersion is

$$\mathrm{d}\Theta = \frac{M}{g\cos\alpha_\mathrm{L}}\,\mathrm{d}\lambda, \tag{3}$$

where M is the magnification of the telescope, α_L the Littrow angle for the particular wavelength and $\mathrm{d}\Theta$ the change in the angle at the VCSEL. For a rough estimation of the angular acceptance $\Delta\Theta$ we take the angular width (HWHM) of the on-axis Fabry–Perot resonance,

$$\Delta\Theta = \sqrt{\frac{n\lambda}{2L_\mathrm{eff}F}}, \tag{4}$$

where F is the finesse of the cold cavity (i.e. without the active medium), which can be estimated from the parameters of the DBRs, n is an average refractive index of the structure and L_eff an effective cavity length (including the penetration of the light field into the DBRs). Combining these two equations, one obtains for the feedback bandwidth

$$\mathrm{d}\lambda = \frac{g\cos\alpha}{M}\sqrt{\frac{n\lambda}{2FL_\mathrm{eff}}}. \tag{5}$$

For the current system $F \approx 2700$, $n \approx 3.4$, $L_\mathrm{eff} \approx 1.2\,\mu$m and hence $\Delta\lambda \approx 0.3$ nm. This is reasonably close to the observed spectral width.

Figure 5 illustrates that the essential features of length scale control do not depend on the geometry of the laser used, but survive in circular lasers, where the excited near field states are standing waves running along the perimeter of the laser [34] because of the current crowding along the perimeter [3].

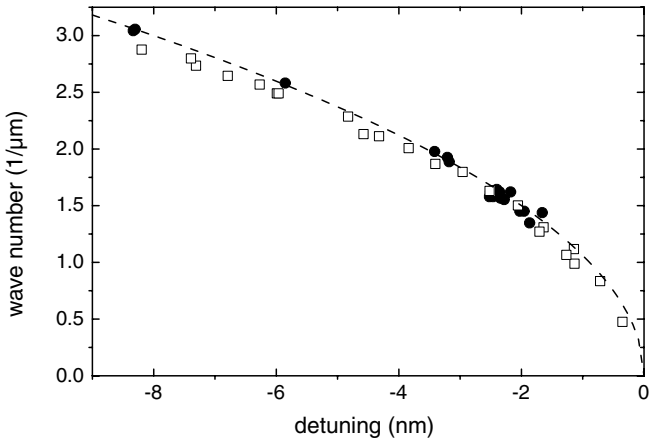

Figure 5. Plot of the dependence of the transverse wave number on detuning to the longitudinal resonance for a circular laser (diameter 80 μm). The solid circles represent the data from the free-running laser, the open squares the ones with feedback. The dashed black line is a fit to the data under free-running conditions (the dispersion curve is different from the one of the square lasers because the epitaxial growth structure is different [34]). Here, an $f = 8$ mm aspheric lens was used for collimation.

Length scale and emission frequency can be tuned over a significant range, the dispersion curve with feedback mirrors the one without feedback and the mode spacing with feedback shows a tendency of being much closer than the one without.

Finally, we mention that a tuning of the length scale is even possible by tilting a plane feedback mirror without an additional frequency-selective element. A range of nearly 3 nm or 1.2 μm^{-1} (without any attempt at optimization) was obtained in a circular VCSEL (200 μm diameter), matching the

dispersion curve obtained with frequency-selective feedback. In tendency, a whole ring of wave vectors is excited as in the case of frequency-selective feedback but there is a significant enhancement of the wave vectors lying in the plane of incidence. We interpret this in the following way: an off-axis wave vector propagating at the angle matching the tilt angle of the mirror is exactly retro-reflected by the mirror (figure 4(*c*)). However, after a round trip the path does not close because the wave vector $\vec{k}_\perp$ is converted to its negative $-\vec{k}_\perp$. Nevertheless, it seems that there is enough linear scattering and nonlinear interaction in the VCSEL to couple two wave vectors with different orientations but the same wave number. A particular important mechanism seems to be the reflection at the oxide boundary because typically we see an enhancement of the effect at the perimeter of the VCSEL, where the returning $-\vec{k}_\perp$ is converted back $+\vec{k}_\perp$, thus closing a feedback loop. Note that the parity is broken in that plane due to the mirror tilt. Hence the emission at components $-\vec{k}_\perp$ and $\vec{k}_\perp$ is not equal any more (unlike in the free-running laser or the laser with feedback from the grating).

4. Experimental results: above threshold states

If the injection current is increased beyond the threshold, the total emitted power and the intensity of the ring in the far field increase. This is expected for a laser above the threshold, of course. In addition, the ring becomes broader and the central wave number increases. The former is due to the excitation of additional transverse modes. The increase in the dominant wave number results from the red-shift of the longitudinal resonance with current: since the feedback wavelength is fixed, the red-shift increases the detuning between longitudinal resonance and feedback and hence the wave number. This change is about $0.03\,\mu\mathrm{m}^{-1}\,\mathrm{mA}^{-1}$ (at $2\,\mu\mathrm{m}^{-1}$) or $-0.05\,\mathrm{nm\,mA}^{-1}$, in good agreement with the current-induced wavelength shift obtained for a single mode of the free-running laser of $0.06\,\mathrm{nm\,mA}^{-1}$.

Figure 6 gives a quantitative account of the broadening of the emission in Fourier space displaying the threshold current for particular wave numbers for different settings of the feedback frequency. The shift of the emission peak (radius of the ring) mentioned above is smaller than $0.1\,\mu\mathrm{m}^{-1}$ in the current range of 3 mA displayed and thus not very evident in the figure.

The central curves (no. 6–2, their minima being around 0.9–$2.3\,\mu\mathrm{m}^{-1}$) are tongue-shaped and fairly sharp. Their width decreases from no. 6 to 2, i.e. with feedback frequency, respectively, wave number. The minimum threshold seems to be independent of the wave number (and hence the wavelength). This is somewhat expected since the semiconductor gain line is much broader than a few nanometres. Indeed, assuming that the feedback efficiency is the same for all configurations, the envelope of the threshold curves should represent the net gain curve (i.e. gain minus losses) of the free-running laser. Hence feedback provides a way to probe that. The fact that the width of the tongues decreases with increasing wave number is probably related to the dispersion curve of the free-running VCSEL: $q^2 \sim \Delta\lambda$, hence $2\delta q q \sim \delta\Delta\lambda$ and $\delta q \sim \delta\Delta\lambda/q$. If the spread in detuning $\delta\Delta\lambda$ is fixed by the feedback selectivity and constant, then the spread in the wave number should indeed decrease with increasing wave number.

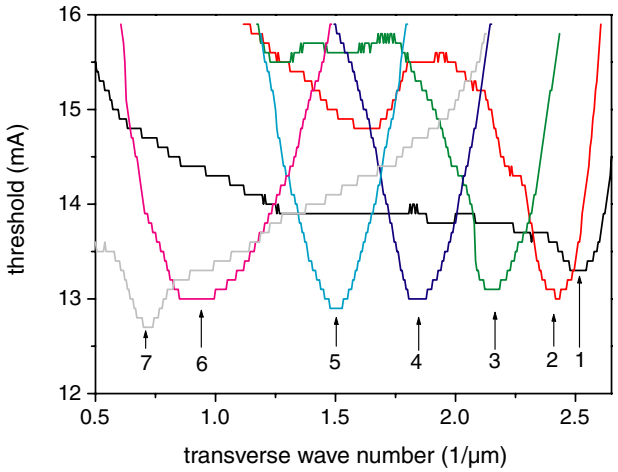

Figure 6. (Colour online) Plot of the dependence of the threshold of emission on the transverse wave number at 20 °C. The curves correspond to different settings of the feedback wavelength. The wavelength is increased in steps of 0.3 nm from black (curve 1) to grey (curve 7), corresponding to a continuous decrease in the favoured wave number.

The two outermost curves (lines 7 and 1, grey and black) are characterized by a small tongue on a much broader background. We do not have an interpretation for that at the moment except that some anomaly might be expected to occur at the end of the tuning intervals. The bumps in curves 2 and 3 (red and green online) far above the threshold are at wave numbers for which the free-running laser shows some preference. It is not unreasonable that there is a fingerprint of that in the spectra with feedback.

However, the result that the net gain curve is quite flat is in strong contrast to the length selection in the free-running laser which shows pinning around a few well-defined wave numbers (see figure 3). This seems to indicate that there is some preference for a few wave numbers (possibly due to parasitic etalon effects in the VCSEL structure) and the excitation of the neighbouring modes is prevented by the clamping of the gain at the threshold gain in a wide range. The feedback here might have been strong enough to wipe out these differences. The preferred wave numbers of the free-running lasers are weakly apparent in the secondary threshold of the feedback case in curves 2 and 3 (red and green online) in figure 6 as indicated before.

5. Measurements with spatial-frequency-selective feedback

In a further step, a spatial filter is inserted in the Fourier plane of the collimating lens. Again, the laser is driven close to the free-running threshold. The polarization-selective optical elements are removed from the feedback beam path to maximize the feedback strength. We first studied the influence of a vertical slit with a width of 2 mm corresponding to a cut-off frequency of $\pm 0.9\,\mu\mathrm{m}^{-1}$.

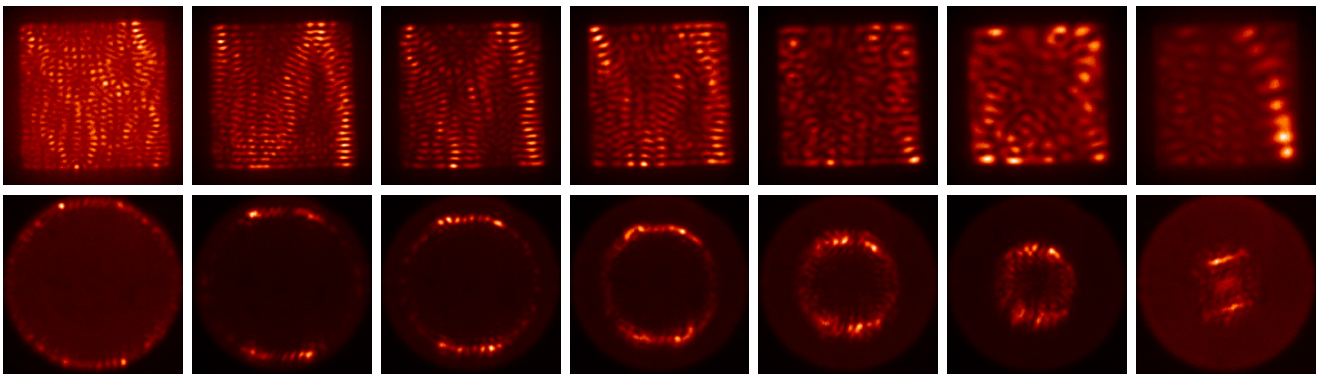

Figure 7. (Colour online) Near-field (upper row) and far-field (lower row) intensity distributions under the influence of frequency-selective feedback combined with Fourier filtering. From left to right the feedback wavelength is increased in steps of about 0.24 nm, corresponding to −120 GHz. The effect of the filtering is most apparent in comparison with figure 2.

Scanning the feedback frequency figure 7 is obtained, which is similar to the previously studied frequency scan in figure 2, but the approximate rotational symmetry present in figure 2 is broken due to the filter: especially in the second and third far-field images the ring is reduced to some spots at the top and at the bottom. The corresponding near-field intensity distribution is much more regular, rather comparable to the wavy stripe patterns observed in the free-running VCSELs [31]. The last two images show nearly no influence of the filter, since the dominant wave number is smaller than 0.9 μm^{-1}, i.e. below the cut-off frequency. For example, the second to last images in figures 2 and 7 are identical. Using a smaller slit width does not change the emitted patterns but only reduces the output power until the laser turns off for a width lower than about half a millimetre.

If a spatial filter is used, which confines strongly not only the angle of the wave vector but also the wave number, explicit frequency selectivity is no longer necessary in the feedback loop due to the correspondence between the wavelength and the wave number. Hence, the grating can be replaced by a highly reflecting mirror in the following experiments. It appears particularly interesting to check whether configurations of wave vectors can be stabilized which are not present in the free-running laser. At the temperatures investigated, the free-running laser emits a structure consisting of four dominant Fourier peaks which are arranged in a rectangle (at 10°) or multiple peaks distributed rather irregularly on a ring (above about 20°; see [31, 35] for examples and a discussion). Numerical simulations though suggest the appearance of a structure consisting of only two peaks in Fourier space corresponding to a stripe pattern aligned parallel to one of the boundaries in the near field [5, 36]. At lower temperatures (wave numbers above about 3.7 μm^{-1}), the laser emits at four dominant peaks arranged in a square on the diagonals in Fourier space. It hence seems interesting to check whether the laser can be forced on a stripe or a square mode. In addition, for applications it is interesting whether emission can be forced to be around zero wave number, i.e. on axis.

The filter used in figures 8(*a*) and (*c*) has two holes of 1 mm diameter, spaced 2 mm horizontally apart corresponding to the centres of the pass band being at ±0.9 μm^{-1}. The centre between the holes is aligned with the optical axis. The resulting

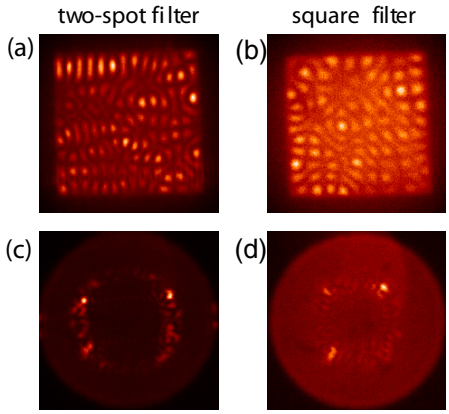

Figure 8. (Colour online) Near-field (*a*) and (*b*) and far-field (*c*) and (*d*) intensity distributions under the influence of spatial-frequency-selective feedback using two different Fourier filters (two holes in the left column; four holes arranged in a square in the right column). Parameters: (*a*) $T = 10\,^{\circ}$C, $I = 17$ mA, 21% above free-running laser threshold. (*b*) $T = 32\,^{\circ}$C, $I = 12.5$ mA, 9% above the free-running laser threshold.

laser emission is not as regular as might be expected: the far field is rather ring-shaped with two to four dominant peaks and a wave number around 1.1 μm^{-1}. The peaks have both a nonzero k_x and k_y, though the filter is designed to force the laser on a mode with $k_y = 0$. The near field is much more regular than comparable images without a filter (cf figure 2) but shows an irregular wavy stripe pattern instead of perfect stripes. This supports the conclusion reached in [31] that these square broad-area VCSELs indeed prefer to lase on four-spot modes rather than on the stripe patterns predicted by numerical simulations [5, 36]. This might be related to the fact that the stripes are particularly sensitive to perturbations in the corners of the oxide waveguide.

In the next experiment, a filter with a square geometry is inserted into the beam path. It consists of four small holes with 0.5 mm diameter, arranged on a square with a side length of 2 mm, corresponding to a transverse mode with a wave number of 1.3 μm^{-1}. In the far field, four weak Fourier components are evident, two of them slightly brighter than the others (figure 8(*d*)). The dominant wave number is 1.0 μm^{-1}, smaller than the one defined by the filter. This is probably

the reason that the emission is comparatively weak. The near-field intensity distribution has a partly square symmetry (figure 8(*b*)), especially in the lower left and upper right corner. This shows that the filter is able to control the shape of the emitted pattern to some extent since the free-running laser would show a four-spot pattern with rectangular symmetry or a ring at these wave numbers.

Finally, we mention that an on-axis filter (i.e. a single hole located on-axis) can be used to select states such as the one on the right-hand side of figure 7 or—depending on alignment—even some states with a maximum on-axis but that the near field remains irregular and filamentary. If the cut-off frequency of the filter is reduced below 0.7 μm^{-1} in an attempt to further enhance the on-axis contribution, the lasers switch off. This illustrates again that homogeneous states interesting for applications cannot be enforced on these lasers.

6. Conclusions

In summary, the tuning of the wave number and the emission wavelength of a broad-area VCSEL over a wide range of 2.5 μm^{-1} and 2.5 nm was demonstrated by using frequency-selective feedback in Littrow configuration. The control works for lasers with square and circular apertures. In this paper, the highest achievable wave number is limited by the NA of the collimating lens used. Hence the system can be improved though we do not expect significant enhancements. The whole range of controllable wave numbers can be shifted to higher wave numbers although by operating at a lower heat sink temperature. The coherence of the lasers is improved but single-frequency operation is not obtained in most cases. The tuning is quasi-continuous demonstrating that the laser states are significantly denser than it appears for the free-running laser. Equation (5) indicates that the bandwidth of the feedback can be reduced—and hence coherence improved—by using a higher resolution grating (e.g. 2400 mm^{-1}) and a higher magnification M. If the latter is achieved via the use of a smaller focal length of the collimating lens, the NA can be improved at the same time. Increasing M by increasing the focal length of the second lens has the disadvantage that the setup becomes significantly larger and more difficult to align. Due to the fact that volume Bragg gratings can have a significantly higher diffraction efficiency (>99%) than diffraction gratings, the feedback strength as well as wavelength selectivity and hence control range and coherence might also be improved by the use of a volume Bragg grating, at least if tuning is not required.

Whereas the control of wave number and wavelength works very fine, experiments on the control of shape and symmetry of the spatial structure by spatial filtering in Fourier space were less successful. This indicates a rather strong preference for certain wave vector configurations, probably because of the transverse boundary conditions in the VCSEL structure (see also [31]). In particular, simple stripes, consisting of two Fourier peaks, suggested as the natural threshold pattern by simulations [5, 36], were never observed in free-running devices and could not be selected by feedback either. In the same way, stabilization of the homogeneous solution (or the fundamental spatial mode of the transverse waveguide) does not seem to be possible. This is probably linked to inhomogeneities but demands further investigation because of the importance in applications.

The envelope of the minimal threshold states for different settings of the feedback frequency is quite flat as expected due to the broadness of the semiconductor gain curve. On the other hand, this is surprising because the free-running laser selects only a few distinct wave numbers if the detuning condition is changed via the heat sink temperature. It might be useful to explore this by reducing the feedback strength and checking at which value of the feedback strength this preference emerges. This would give an indication of the net gain variations. This result should then be checked against more conventional approaches to measure gain differences as looking at the below threshold resonances (e.g. by adapting methods developed for the longitudinal modes of edge-emitting lasers, e.g. [37]).

Acknowledgments

This work was supported by the Deutsche Forschungsgemeinschaft and by the STREP FunFACS of the European Union. The collaboration between the groups was supported by the British Council, the Deutsche Akademische Austauschdienst and the Taiwanese Research Council. The authors are grateful for useful discussions with I Babushkin and P Paulau.

References

[1] Revermann M, Timmermann A, Meinschien J and Bruns P 2007 Efficient high-brightness diode laser modules offer new industrial applications *Proc. SPIE* **6456** 64560Q
[2] Grabherr M, Jäger R, Miller M, Thalmaier C, Herlein J and Ebeling K J 1998 Bottom-emitting VCSELs for high-CW optical output power *IEEE Photon. Technol. Lett.* **10** 1061–3
[3] Grabherr M, Miller M, Jäger R, Michalzik R, Martin U, Unold H J and Ebeling K J 1999 High-power VCSEL's single devices and densely packed 2-D-arrays *IEEE J. Sel. Top. Quantum Electron.* **5** 495–502
[4] Hess O 1998 Spatio-spectral dynamics and spontaneous ultrafast optical switching in VCSEL arrays *Opt. Express* **2** 424–30
[5] Rössler T, Indik R A, Harkness G K and Moloney J V 1998 Modeling the interplay of thermal effects and transverse mode behavior in native-oxide confined vertical-cavity surface-emitting lasers *Phys. Rev.* A **58** 3279–92
[6] Moloney J V 1999 Spontaneous generation of patterns and their control in nonlinear optical systems *J. Opt. B: Quantum Semiclass. Opt.* **1** 183–90
[7] Fischer I, Hess O, Elsäßer W and Göbel E 1997 Complex spatio-temporal dynamics in the near-field of a broad-area semiconductor laser *Europhys. Lett.* **35** 579–84
[8] Hadley M A, Wilson G C, Lau K Y and Smith J S 1993 High single-transverse mode output from external-cavity surface-emitting laser diodes *Appl. Phys. Lett.* **63** 1607–9
[9] Hochheiser D, Moloney J V and Lega J 1997 Controlling optical turbulence *Phys. Rev.* A **55** R4011–4
[10] Cassetari D, Arimondo E and Verkerk P 1998 External-cavity broad-area laser diode operating on the D_1 line of cesium *Opt. Lett.* **23** 1135–7
[11] Lobel M, Petersen P M and Johansen P M 1998 Single-mode operation of a laser-diode array with frequency-selective phase-conjugate feedback *Opt. Lett.* **23** 825–7

[12] Simmendinger C, Preißer D and Hess O 1999 Stabilization of chaotic spatiotemporal filamentation in large broad area lasers by spatially structured optical feedback *Opt. Express* **5** 48–54
[13] Wolff S, Messerschmidt D and Fouckhardt H 1999 Fourier-optical selection of higher order transverse modes in broad area lasers *Opt. Express* **5** 32–6
[14] Raab V, Skoczowsky D and Menzel R 2002 Tuning high-power laser diodes with as much as 0.38 W of power and $M^2 = 1.2$ over a range of 32 nm with 3 GHz bandwidth *Opt. Lett.* **27** 1995–7
[15] Mandre S K, Fischer I and Elsäßer W 2003 Control of the spatiotemporal emission of a broad-area semiconductor laser by spatially filtered feedback *Opt. Lett.* **28** 1135–7
[16] Reboud V, Dubreuil N, Fournet P, Pauliat G and Roosen G 2006 Self-induced transverse mode selection in a photorefractive extended cavity laser diode *Opt. Express* **14** 2735–43
[17] Jensen O B, Thestrup B, Andersen P E and Petersen P M 2006 Near-diffraction-limited segmented broad area diode laser based on off-axis spectral beam combining *Appl. Phys.* B **83** 225–8
[18] Tierno A and Ackemann T 2007 Tunable, narrow-band light source in the 1.25 μm region based on broad-area quantum dot lasers with feedback *Appl. Phys.* B **89** 585–8
[19] Maiwald M, Ginolas A, Müller A, Sahm A, Sumpf B, Erbert G and Tränkle G 2008 Wavelength-stabilized compact diode laser system on a microoptical bench with 1.5 W optical output power at 671 nm *IEEE Photon. Technol. Lett.* **20** 1627–9
[20] Marino F, Barland S and Balle S 2003 Single-mode operation and transverse-mode control in vcsels induced by frequency-selective feedback *IEEE Photon. Technol. Lett.* **15** 789–91
[21] Tanguy Y, Ackemann T and Jäger R 2006 Characteristics of bistable localized emission states in broad-area vertical-cavity surface-emitting lasers with frequency-selective feedback *Phys. Rev.* A **74** 053824
[22] Tanguy Y, Ackemann T, Firth W J and Jäger R 2008 Realization of a semiconductor-based cavity soliton laser *Phys. Rev. Lett.* **100** 013907
[23] Park H M and Sung M C 2003 Stabilization of two-dimensional Rayleigh–Bénard convection by means of optimal feedback control *Physica* D **186** 185–204
[24] Martin R, Oppo G-L, Harkness G K, Scroggie A J and Firth W J 1997 Controlling pattern formation and spatio-temporal disorder in nonlinear optics *Opt. Express* **1** 39–43
[25] Mamaev A V and Saffman M 1998 Selection of unstable patterns and control of optical turbulence by Fourier plane filtering *Phys. Rev. Lett.* **80** 3499–503
[26] Jensen S J, Schwab M and Denz C 1998 Manipulation, stabilization and control of pattern formation using Fourier space filtering *Phys. Rev. Lett.* **81** 1614–7
[27] Ackemann T, Giese B, Schäpers B and Lange W 1999 Investigation of pattern forming mechanisms by Fourier filtering properties of hexagons and the transition to stripes in an anisotropic system *J. Opt. B: Quantum Semiclass. Opt.* **1** 70–6
[28] Harkness G K, Oppo G-L, Benkler E, Kreuzer M, Neubecker R and Tschudi T 1999 Fourier space control in an LCLV feedback system *J. Opt. B: Quantum Semiclass. Opt.* **1** 177–82
[29] Jakobsen P K, Moloney J V, Newell A C and Indik R 1992 Space-time dynamics of wide-gain-section lasers *Phys. Rev.* A **45** 8129–37
[30] Schulz-Ruhtenberg M, Babushkin I V, Loiko N A, Ackemann T and Huang K F 2005 Transverse patterns and length-scale selection in vertical-cavity surface-emitting lasers with a large square aperture *Appl. Phys.* B **81** 945–53
[31] Babushkin I V, Schulz-Ruhtenberg M, Loiko N A, Huang K F and Ackemann T 2008 Coupling of polarization and spatial degrees of freedom of highly divergent emission in broad-area square vertical-cavity surface-emitting lasers *Phys. Rev. Lett.* **100** 213901
[32] Hegarty S P, Huyet G, McInerney J G and Choquette K D 1999 Pattern formation in the transverse section of a laser with a large Fresnel number *Phys. Rev. Lett.* **82** 1434–7
[33] Palmer C and Loewen E 2005 *Diffraction Gratings Handbook* 6th edn Newport Corp. http//gratings.newport.com/information/handbook/handbook.asp
[34] Schulz-Ruhtenberg M 2008 Experimental analysis of spatial states in broad-area vertical-cavity surface-emitting lasers *PhD Thesis* Westfälische Wilhelms-Universität Münster http://nbn-resolving.de/um:nbn:de:hbz:6-14549409755
[35] Huang K F, Chen Y F, Lai H C and Lan Y P 2002 Observation of the wave function of a quantum billiard from the transverse patterns of vertical cavity surface emitting lasers *Phys. Rev. Lett.* **89** 224102
[36] Loiko N A and Babushkin I V 2001 Competition of orthogonally polarized transverse Fourier modes in a VCSEL *J. Opt. B: Quantum Semiclass. Opt.* **3** S234–43
[37] Hakki B W and Paoli T L 1973 Cw degradation at 300° of GaAs double-heterostructure junction lasers: II. Electronic gain *J. Appl. Phys.* **44** 4113–9